Structure–Property Relationship of Polyethylene Glycol-Based PU/PAN Semi-Interpenetrating Polymer Networks

H. Kumar,[1] Siddaramaiah,[2] R. Somashekar,[3] S. S. Mahesh,[3] S. Abhishek,[3] T. N. Guru Row,[4] Geetha S. Kini [4]

[1]*Department of Chemistry, R.V. College of Engineering, Bangalore 560 059, India*
[2]*Department of Polymer Science and Technology, Sri Jayachamarajendra College of Engineering, Mysore 570 006, India*
[3]*Department of Studies in Physics, University of Mysore, Mysore 570 006, India*
[4]*Department of Solid State and Structural Chemistry, Indian Institute of Science, Bangalore 560 001, India*

Received 26 February 2005; accepted 26 April 2005
DOI 10.1002/app.22147
Published online in Wiley InterScience (www.interscience.wiley.com).

ABSTRACT: Polyethylene glycol-400 (PEG) based polyurethane (PU) and polyacrylonitrile (PAN) semi-interpenetrating polymer networks (SIPNs) (PU/PAN; 90/10, 70/30, 60/40, and 50/50) have been prepared by sequential polymerization method. The prepared SIPNs have been characterized by physicomechanical properties. The microcrystalline parameters such as crystal size ($\langle N \rangle$), lattice disorder (g), surface (D_s) and volume (D_v) weighted crystal size of SIPNs have been estimated using wide angle X-ray scattering studies, and quantification of the polymer network has been carried out on the basis of these parameters. The microstructural parameters have been established using Exponential, Lognormal, and Reinhold asymmetric column length distribution functions and the results are compiled. © 2005 Wiley Periodicals, Inc. J Appl Polym Sci 99: 177–187, 2006

Key words: polyurethane; PU/PAN; IPNs; WAXS; microcrystalline parameters

INTRODUCTION

Interpenetrating polymer networks (IPNs), which are specialty blends, have attracted attention in the last two decades[1–6] because of their versatility and wide spectrum of properties. Interpenetrating polymerization is a mode of blending two polymers to produce a mixture in which phase separation is not as extensive as it would be otherwise.[7] IPNs synthesized so far exhibit various degrees of phase separation depending mainly on the miscibility of polymers.[8–16] Hourston and coworkers[8–10] carried out a detailed investigation of the synthesis and properties of various polyurethane/polyacrylate IPNs. The synthesis and characterization of castor oil-based polyurethane (PU) IPNs have been studied by different groups.[14–17] Many researchers have found that polyethylene glycol-based PUs and its IPNs are biocompatible and some are biodegradable.[18–20] These materials are being used in the manufacturing of scaffolds, pacemakers, and self-healing bandages.[21–22] Many researchers have studied characterization of PU or IPNs using wide angle X-ray scattering.[23–25] The present study is an effort to interpret the X-ray pattern and observed property of PU/PAN IPNs using three different models such as Exponential, Lognormal, and Reinhold asymmetric column length distribution functions. Since each of the Bragg reflections in these samples, referred as (*hkl*) reflection, are broadened because of crystal imperfections, we have used profile analysis technique to quantify these imperfections. Normally, the broadening of a profile arises as a result of limited number of unit cells $\langle N \rangle$ called crystal size, counted in a direction perpendicular to Bragg planes (*hkl*) and a disorder of second kind, referred as lattice strain (g, in %). This is given by $\Delta d/d$, where Δd is change in the interplanar spacing and d is the interplanar spacing.

Correspondence to: Siddaramaiah (siddaramaiah@yahoo.com).

Journal of Applied Polymer Science, Vol. 99, 177–187 (2006)

EXPERIMENTAL

Materials

Polyethylene glycol-400 (PEG) (Ranbaxy Laboratories, India), benzoyl peroxide (Aldrich, Milwaukee, WI), and 4,4′-diphenyl methane diisocyanate (MDI) (Merck, Whitehouse Station, NJ) were used as such. Acrylonitrile (SD Fine Chem Ltd., Boisar, India) monomer was freed from the stabilizer prior to use.

Synthesis

Polyurethane (PU) was prepared using 1 : 1.5 mol of PEG and MDI in the presence of 0.05% new catalyst.[26] The different weight ratios of acrylonitrile with 0.5% of benzoyl peroxide were added to the reaction mixture. The mixture is stirred thoroughly for 30 min at

TABLE I
Physicomechanical Properties of PU/PAN IPNs

% formulation of PU/PAN (wt/wt)	Solubility parameter $(cal/cm^3)^{1/2}$	Density ± 0.1% (g/cc)	Density, theoretical (g/cc)	Specific tensile strength (MPa/(g/cm^3))	Tensile modulus (MPa)
90/10	13.720	1.232	1.238	4.87	13.58
73/30	13.414	1.228	1.224	5.21	18.87
60/40	13.262	1.224	1.217	3.35	5.09
50/50	13.110	1.218	1.210	3.45	5.09

room temperature to get homogeneous solution of prepolyurethane. Then the reaction mixture is poured into a cleaned glass mold sprayed with releasing agent in a closed chamber. The mold was kept at room temperature for 24 h for PU formation. Then, the temperature of the mold was slowly raised to 80°C to polymerize acrylonitrile by sequential polymerization.[27,28] The transparent golden yellow to brown colored PU/PAN IPNs were taken out of the mold.

Physicomechanical properties

Mechanical properties, like tensile behavior, was measured as per ASTM D-882 method using a 4302 model Hounsfield Universal testing machine (UTM) H50 KM, UK. A minimum of six samples was tested for each composition and the average value has been reported. Density was measured as per ASTM D-792–86 method.

Swelling behavior

The IPNs were cut into circular pieces, weighed accurately, and immersed in benzene, toluene, and xylene solvents to attain equilibrium. The samples were then taken out from the solvent bath, wiped with tissue paper to remove adhered solvents, and weighed immediately. The percentage swelling was calculated for each IPNs.[29]

$$Swelling\ (\%) = (weight\ of\ swollen\ polymer - weight\ of\ dry\ polymer)/weight\ of\ dry\ polymer \quad (1)$$

From the equilibrium swelling data, the molecular mass between crosslinks can be calculated using the equation[30,31]

$$M_c = -\rho_p V_s \Phi^{1/3} / [\ln(1-\Phi) + \Phi + \chi\Phi^2] \quad (2)$$

where ρ_p is the density of polymer, V_s is the molar volume of solvent, Φ is the volume fraction of polymer and χ is the interaction parameter.

The volume fraction of polymer Φ in the swollen sample was calculated using the equation

$$\phi = \frac{W_1/\rho_p}{[(W_1/\rho_p) + (W_2/\rho_s)]} \quad (3)$$

where, W_1 is weight of polymer and ρ_p the density of polymer, W_2 the weight of solvent in the swollen sample, and ρ_s the density of solvent.

The interaction parameter χ is given by the equation[30]

$$\chi = \frac{(\beta + V)}{[RT(\delta_A - \delta_B)^2]} \quad (4)$$

where, V is the molar volume of solvent, δ_A and δ_B are the solubility parameters of solvent and polymer, respectively, R is the universal gas constant, and T is the absolute temperature. β the lattice constant is equal to 0.34. From the M_c value, the crosslink density (V_e) and degree of crosslinking (V) can be calculated using the equation[32]

$$V_e = \rho_p/M_c \quad (5)$$

TABLE II
Percentage Swelling of IPNs in Aromatic Solvents

Solvent	Solubility parameter $(cal/cm^3)^{1/2}$	Molar volume (cm^3/mol)	Percentage swelling of IPN with PAN content			
			10%	30%	40%	50%
Benzene	9.2	88.74	17.05	16.50	22.20	13.56
Toluene	8.9	106.5	5.44	7.86	9.75	7.54
p-Xylene	8.8	123.1	3.42	3.65	3.52	4.16

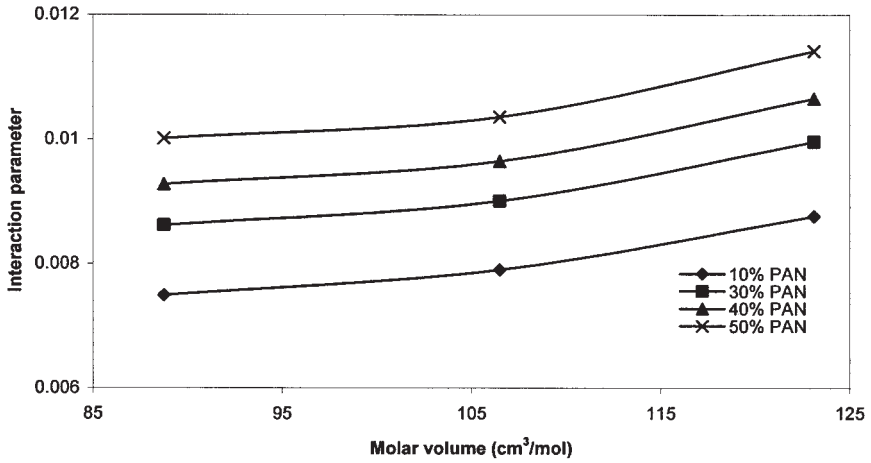

Figure 1 Interaction parameter of IPN-solvent systems with respect to molar volume of solvents.

$$V = 1/(2M_c) \quad (6)$$

X-ray powder pattern recording and analysis

X-ray powder pattern of IPNs were recorded using a Philips PW 1140 diffractometer of Bragg–Branto Geometry (fine focus setting) with germanium monochromatic radiation of Co Kα (λ = 0.1542 nm) for 2θ range 5–50 at intervals of 0.03, employing a curved position sensitive detector (CPSD) in the transmission mode. These patterns were indexed using TREOR procedure. The intensity was corrected for Lorentz-polarization factors and also for instrumental broadening using Stokes deconvolution method.[33]

Microstructural parameters like crystal size $\langle N \rangle$ and lattice strain (g, in %) are usually determined by employing the Fourier method of Warren and Averbach.[34–36] The intensity of a profile in the direction joining the origin to the center of the Bragg reflection can be expanded in terms of the Fourier cosine series as

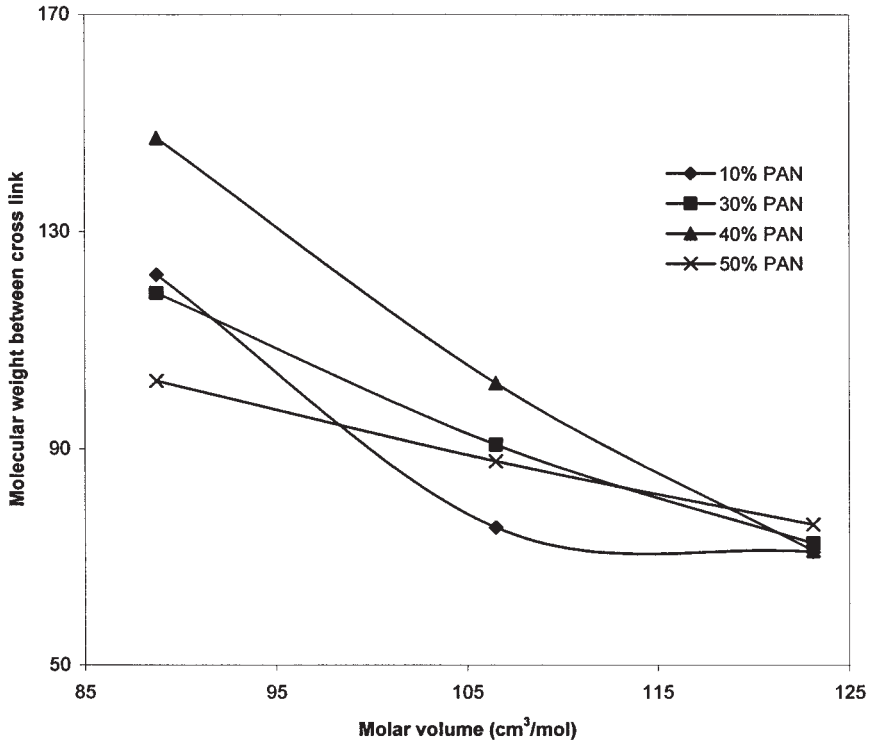

Figure 2 Molecular weight between crosslink with respect to molar volume solvents.

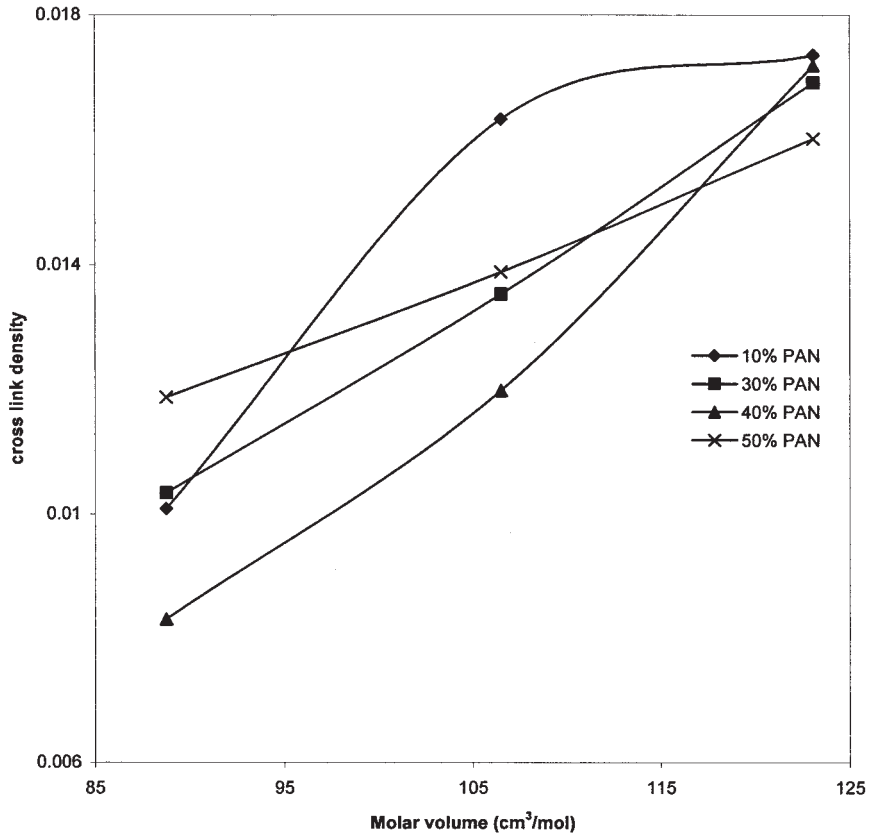

Figure 3 Cross link density exhibited by polymer network with respect to molar volume of solvents.

$$ls = \sum_{n=-\infty}^{\infty} A(n)\cos\{2\pi nd \quad (s - s_0)\} \tag{7}$$

where, $A(n)$ is the product of size coefficients A_s(n) and lattice distortion (strain coefficient) A_d(n). Here, s is $\sin(\theta/\lambda)$, n is the harmonic number and d is the lattice spacing. The Fourier coefficients can be expressed as

$$A(n) = As(n)Ad(n) \tag{8}$$

For any Parcrystalline material, like polymer, $A_d(n)$ turns out to be[36,37]

$$A_d(n) = \exp(-2\pi^2 m^2 ng^2) \tag{9}$$

For a probability distribution of column lengths $P(i)$, we have

$$A_s(n) = 1 - \frac{nd}{D} - \frac{d}{D}\left[\int_o^n iP(i)di - n\int_0^n P(i)di\right] \tag{10}$$

where, $D = \langle N\rangle d_{hkl}$ is the crystallite size and i is the number of unit cells in a column. In the presence of two orders of reflections from the set of Bragg planes, Warren and Averbach[34] have shown a method of obtaining the crystal size ($\langle N\rangle$) and lattice strain (g, in %). But in polymers it is very rare to find multiple reflections. So, to find the finer details of microstructure, we have considered only asymmetric functions. Another advantage of this method is that the distribution function is different along different directions. However, Ribarik et al.,[38] Popa et al.,[39] and Scardi et al.[40] have used a single crystal size distribution function for the whole pattern fitting, which we feel, may be inadequate to describe polymer diffraction patterns, but adequate enough to quantify the stacking faults in metal oxide compounds. Here, we would like to emphasize that the Fourier method of profile analysis (single-order method used here) is a quite reliable one as per the recent survey and results of Round Robin test conducted by IUCr.[41] In fact for refinement, we have considered the effect of background by introducing a parameter.[42] We have used three asymmetric (Exponential, Lognormal, and Reinhold) column length distribution functions for the computation of microstructural parameters.

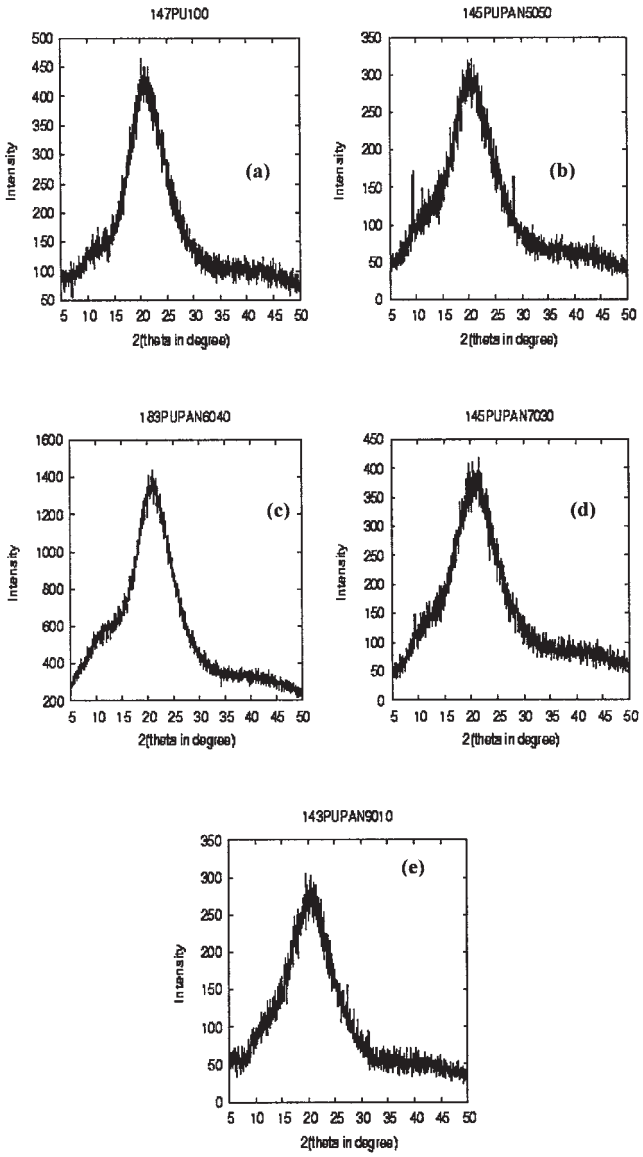

Figure 4 X-ray Patterns of (a) 100/00, (b) 50/50, (c) 60/40, (d) 70/30, and (e) 90/10 PU/PAN IPNs.

Note that these equations are used for the analysis of single-order reflections usually observed in fiber X-ray diffraction. This can also be used to yield more accurate results when two or more orders of reflections are available.

The lognormal distribution

The lognormal-size distribution density function is given by

$$P(i) = \frac{1}{(2\pi)^{1/2}\sigma}\frac{1}{i}\exp\left\{-\frac{[\log(i/m)]^2}{2\sigma^2}\right\} \qquad (15)$$

where, σ is the variance and m is the median of the distribution.

Substituting the above equation in eq. (10) and simplifying,[38] we get the equation for size coefficients as

$$As(n) = \frac{m^3\exp[(9/4)(2^{1/2}\sigma)^2]}{3} erfc \times \left[\frac{log(|n|/m)}{2^{1/2}\sigma} - \frac{3}{2}2^{1/2}\sigma\right] - \frac{m^2\exp(2^{1/2}\sigma)^2}{2}|n| erfc \times \left[\frac{log(|n|m)}{2^{1/2}\sigma} - 2^{1/2}\sigma\right] + \frac{|n|^3}{6} erfc\left[\frac{\log(|n|/m)}{2^{1/2}\sigma}\right] \qquad (16)$$

The exponential distribution

It is assumed that there are no columns containing fewer than p unit cells but that the numbers of those longer than this decay exponentially. Thus, we have[43]

$$P(i) = \begin{cases} 0 & \text{if } p < i \\ \alpha\exp\{-\alpha(i-p)\} & \text{if } p \geq i \end{cases} \qquad (11)$$

where, $\alpha = 1/(N-p)$. Substituting this in eq. (9), we get

$$A_s(n) = \begin{cases} A(0)(1 - n/<N>) & \text{if } n \leq p \\ A(0)\{\exp[-\alpha(n-p)]\}/(\alpha N) & \text{if} n \geq p \end{cases} \qquad (12)$$

where, α represents width of the distribution, which has been varied to fit the experimental results. p is the smallest number of unit cells in a column, [lrang]$\langle N\rangle$ is the number of unit cells counted in a direction perpendicular to the (*hkl*) Bragg plane, d is the spacing of the (*hkl*) planes, λ is the wavelength of X-rays used, D_s is the surface weighted crystal size $D = <N>d_{hkl}$.

Reinhold distribution

With the exponential distribution function, $P(i)$ rises discontinuously at p, from zero to its maximum value.[43,44] In contrast, the Reinhold function allows a continuous change by putting

$$P(i) = \begin{cases} 0 & \text{if } i \leq p \\ \beta^2(i-p)\exp\{-\beta(i-p)\} & \text{if } i > p \end{cases} \qquad (13)$$

where, $\beta = 2/(N - P)$. Substituting this in eq. (10), we get

$$A_s(n) = \begin{cases} A(0)(1 - n/<N>) & \text{if } n \leq p \\ [A(0)(n - p + 2/\beta)/N]\{\exp[-\beta(n-p)]\} & \text{if } n \geq p \end{cases} \qquad (14)$$

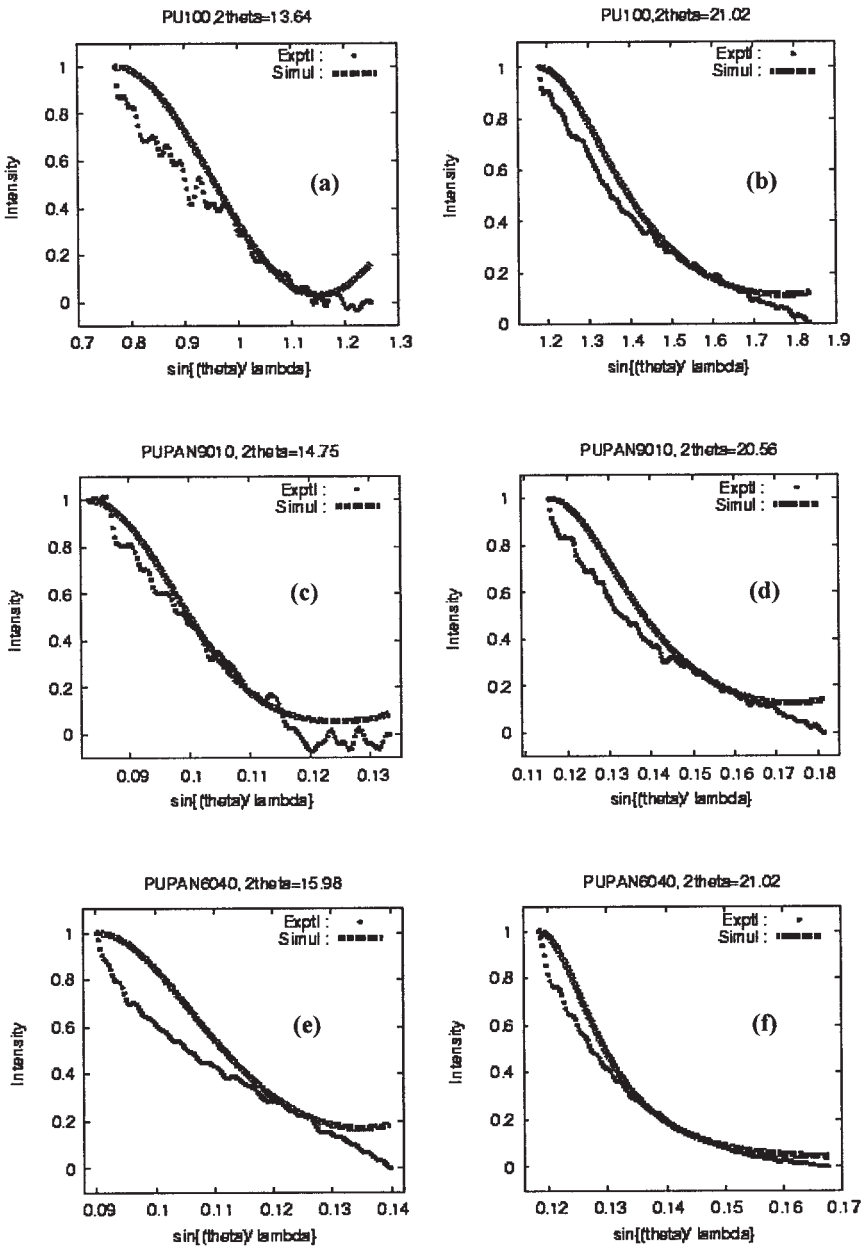

Figure 5 Experimental and simulated X-ray profiles for (a,b) 100/00, (c,d) 90/10, (e,f) 60/40, (g,h) 50/50, and (i,j) 70/30 PU/PAN IPNs using exponential distribution functions at two different 2θ values.

The surface weighted mean column length $\langle N \rangle_{\text{surf}}$ is given by

$$< N >_{\text{surf}} = \frac{2m \exp[(5/4)(2^{1/2}\sigma)^2]}{3} \qquad (17)$$

and the volume weighted column length $\langle N \rangle$ is given by

$$< N >_{\text{vol}} = \frac{3m \exp[(7/4)(2^{1/2}\sigma)^2]}{4} \qquad (18)$$

RESULTS AND DISCUSSION

Physicomechanical properties

The measured physicomechanical properties of PU-based IPNs are given in Table I. The density of PU is 1.245 g/cc and its IPNs lies in the range of 1.218–1.232 g/cc and these values are in the expected range. The densities of IPNs have also been calculated theoretically by additive method and obtained values are given in Table I. The theoretically calculated values are comparable with experimental results. In Table I it was observed that there was no systematic variation in

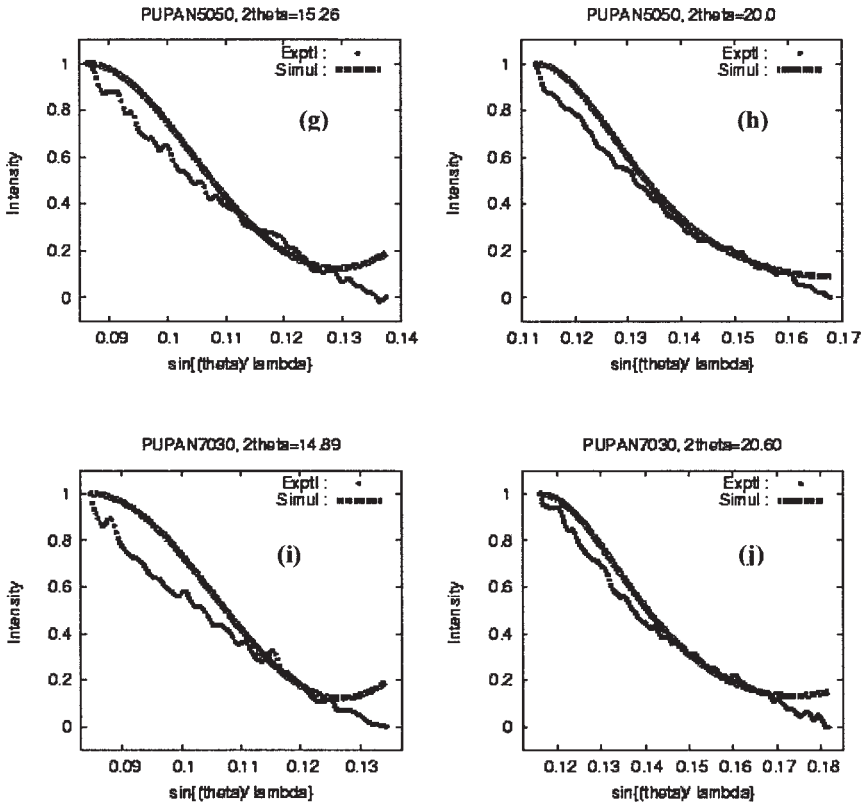

Figure 5 (*Continued from the previous page*)

elastic modules with the compositions of PU/PAN systems and it lies in the range of 5.09–18.87 MPa. Higher moduls has been observed for 70/30 PU/PAN.[45] The higher tensile properties with 30% PAN content imply a higher degree of physical entanglement and hydrogen bond formation between PU and PAN network. This would result in an effective transfer of stress between two polymer components of IPN, thus leading to enhancement in mechanical strength and retaining of percentage elongation upon tensile deformation. The physical entanglement is most likely due to the formation of bicontinous phase at a critical acrylonitrile composition. Suthar et al.[45] and Susheela Bai et al.[46] noticed similar trends with PU IPNs. The specific tensile strength lies in the range of 3.35–5.21 MPa/(g/cm^3).

Swelling behavior

The percentage swelling of benzene, toluene, and *p*-xylene into IPNs are given in Table II. From the Table it is evident that as the molar volume of penetrant increases the percentage swelling decreases. This indicates that the solvent uptake into IPN depends on size or molar volume of penetrant. Among the IPNs, 60/40 PU/PAN shows a higher degree of swelling than other IPNs for all penetrants. However, relatively bulkier *p*-xylene shows almost the same degree of swelling in all IPNs. The variation of χ values for all IPNs is compared with molar volume of solvents and is shown in Figure 1. Interaction parameter is found to increase with the increase of PAN content in IPNs. This is probably due to an increase in highly polar PAN content in polar PU matrix. This synergic effect may increase the interaction. The molecular mass between the interlocking (crosslinking) obtained from eq. (2) is found to vary with molar volume of solvents. As the molar volume increases, the molecular mass between crosslink decreases.[47] This is on the expected lines.

The calculated M_c and V are plotted as a function of molar volume of solvent in Figures 2 and 3, respectively. As the molar volume of solvents increases, crosslink density increases and thus molecular mass between interlocking decreases and *vice versa*. For a given solvent system, 60/40 PU/PAN exhibit lower crosslink density than other IPNs. Hence, M_c for 60/40 PU/PAN is higher than that for other members of the family.

X-ray powder pattern analysis

The IPNs were analyzed by X-ray studies and the obtained diffractogram for all IPNs are shown in Figures 4(a–c). X-ray studies indicate the increase in crystalline region with increase of PAN. This is possible

only with increase in hydrogen bonds between polymer chains, leading to a more ordered segment in a wider polymer network. Equatorial scan of the X-ray reflection profile obtained from polyethylene glycol-based PU/PAN polymers was used for the estimation of microcrystalline parameters such as crystal size ($\langle N \rangle$) and lattice distortion (g, in %). As mentioned earlier, all the distribution functions were put to test to find out the most suitable crystal size distribution function for the profile analysis of the X-ray fiber diffraction. The procedure adopted for the computation of the parameters is as follows. Initial values of g and $\langle N \rangle$ were obtained using the method of Nandi et al.[48] These values were used in the equations mentioned earlier in the text to give the corresponding values for the width of distribution. These are only rough estimates, and so the refinement procedure must be sufficiently robust to start with such values. Here, we compute

$$\Delta^2 = [I_{cal} - (I_{exp} + BG^2]^2/\text{Number of points} \quad (19)$$

where, BG is the error in the background estimation. The values of Δ were divided by half the maximum value of intensity so that it is expressed relative to the mean value of intensities, and then minimized. For refinement against intensities, the multidimensional minimization algorithm of the SIMPLEX method was used.[49] In all the cases the goodness of the fit was less than 15%. Figure 5(a–j) shows experimental and simulated x-ray profiles for PU and PU/PAN IPNs using exponential distribution functions at different 2θ values. It is evident from this figure that there is a good agreement between experimental and calculated X-ray data. The microcrystalline parameters used for simulating the X-ray profiles are given in Table III, using various asymmetric distribution functions. From Table III, it is evident that exponential distribution has less standard deviation compared to other distribution functions and hence, we have used the corresponding results for further interpreting the results. We observe from these tables that with increase in PU, the crystallite size increases, which is in agreement with the observations made by Lee et al. elsewhere.[50] We have used the computed microstructural parameters for computing the shape of the coherent domains in terms of the shape of the ellipsoid by taking the surface weighted crystal size (D_s) values, corresponding to average 2θ values along x and y axis, respectively, and the same is shown in Figure 6. From this figure it is evident that there are significant changes only in the periphery of the crystallite shape ellipsoid. The variation of tenacity with crystallite size for these IPNs is shown in Figure 7. The tenacity value of the IPNs increases with increase in crystallite size and also with increase in PU concentration. This increase in crystallite size with PU can be associated to co-operative

TABLE III
Microstructural Parameters for PU/PAN IPNs by Asymmetric Column Length Distribution Functions

Composition of PU/PAN	2θ (°)	g (%)	D_s (Å)	D_v (Å)	$\langle N \rangle$	δ
Exponential distribution						
50/50	15.26	4.0	14.37	15.03	1.73	0.07
	20.00	5.0	14.37	14.83	2.11	0.03
60/40	15.98	4.0	12.87	14.11	1.66	0.07
	21.02	5.0	23.37	25.65	3.39	0.04
70/30	14.89	1.4	9.94	9.96	1.65	0.07
	20.60	4.0	12.80	13.36	1.81	0.05
90/10	14.75	4.0	17.91	18.05	2.24	0.07
	20.56	5.0	13.34	14.02	1.90	0.05
100/00	13.64	5.0	16.29	16.31	2.03	0.06
	21.02	4.0	13.33	14.10	1.95	0.04
Reinhold distribution						
50/50	15.26	0.5	16.71	17.40	1.68	0.06
	20.00	5.0	15.16	16.06	2.10	0.03
60/40	15.98	1.5	14.79	16.26	1.63	0.07
	21.02	2.0	22.70	26.61	3.10	0.04
70/30	14.89	5.5	13.69	14.26	1.71	0.06
	20.60	1.0	13.79	14.65	1.76	0.05
90/10	14.75	0.5	17.28	17.43	2.20	0.06
	20.56	1.5	14.40	15.60	1.81	0.05
100/00	13.64	0.5	13.12	13.18	1.93	0.06
	21.02	1.5	14.43	15.73	1.90	0.04
Lognormal distribution						
50/50	15.26	0.5	9.06	10.22	1.76	0.06
	20.00	5.0	8.75	9.81	2.21	0.04
60/40	15.98	0.5	8.49	9.59	1.73	0.07
	21.02	0.5	13.57	15.26	3.61	0.06
70/30	14.89	1.0	8.98	10.11	1.71	0.06
	20.60	0.5	7.24	8.15	1.90	0.05
90/10	14.75	0.5	11.83	13.27	2.21	0.09
	20.56	0.5	7.60	8.51	1.97	0.05
100/00	13.64	0.5	11.10	12.46	1.92	0.08
	21.02	0.5	7.69	8.69	2.05	0.05

movements of the molecular chains that form the amorphous and interfacial regions. Such movements trigger motions in the crystalline phase, which result in increase in crystallite size. Transparency of these IPNs also suggests the applicability of these materials in packing or coating industries. These studies also emphatically indicate that an increase of PU in PU/PAN IPNs leads to overall increase in weak inter and intrahydrogen bonds between —NHCOO—, C—O—C groups of PU with —CN group of PAN and dipole–dipole interactions, which are essential for the formation of polymer network. It is also observed from these calculations that the changes in the paracrystalline disorder (termed as lattice strain) in PU/PAN IPNs are significantly small but do contribute for broadening of the X-ray profiles, which we have quantified in this article.

CONCLUSIONS

The tensile property of 70/30 PU/PAN is maximum, which is due effective entanglement of polymer net-

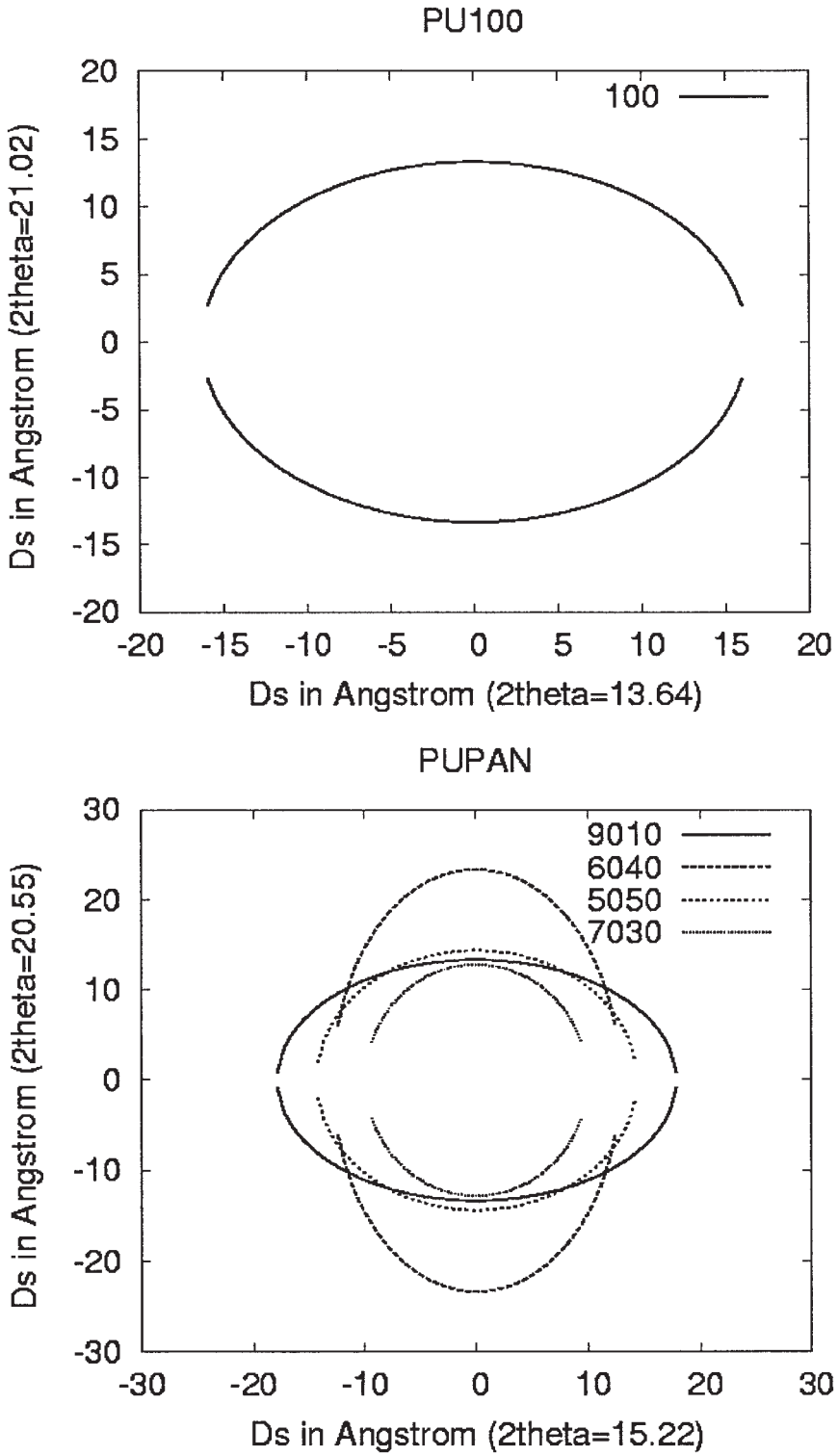

Figure 6 Cxystallite shape ellipsoid for PU and PU/PAN IPNs.

work. X-ray studies indicate the increase in crystalline region with increase of PAN in PU/PAN IPNs. This is possible only with increase in hydrogen bonds between polymer chains, leading to a more ordered segment in a wider polymer network. These structural modifications are in agreement with the empirical properties such as variation of molecular weight between crosslinks with molar volume of solvents, interaction parameters, and crosslink density. Changes in swelling behavior with solvents were noticed in these IPNs because of complicated chemical structure and morphology. Microstructural parameters of IPNs

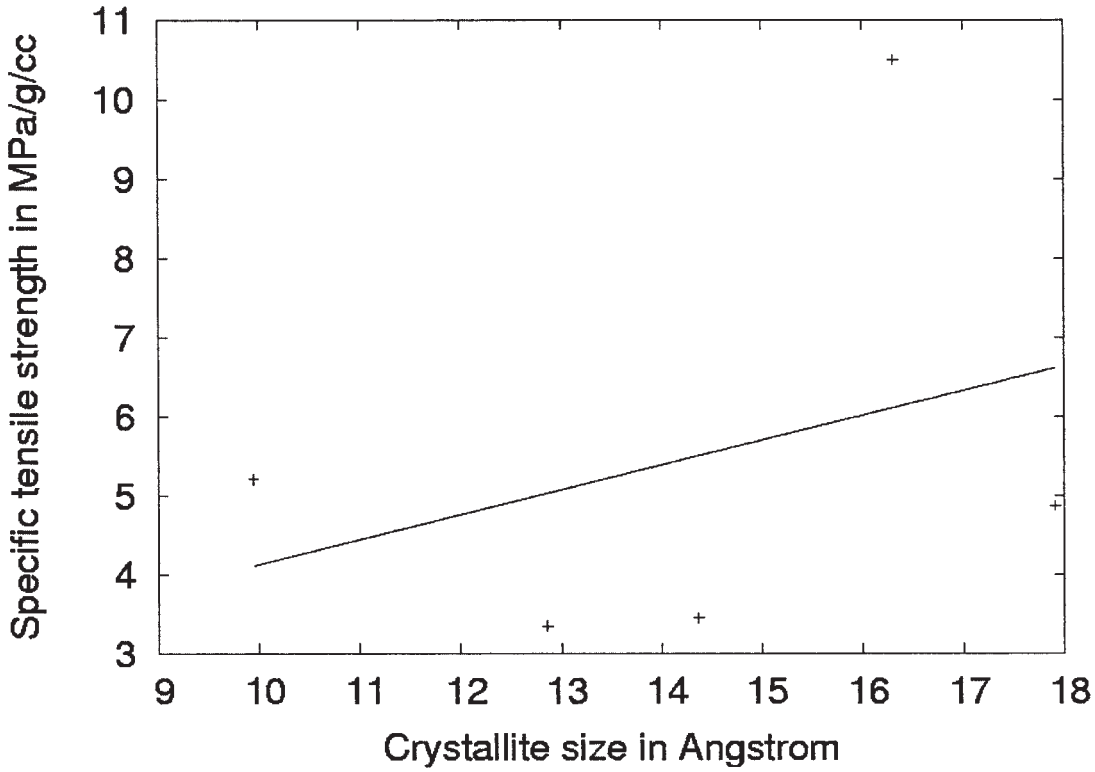

Figure 7 Plot of specific tensile strength versus crystallite size.

do justify these observations and the crystallite shape ellipsoid shows peripheral changes with increase of PAN in PU/PAN IPNs. Exponential distribution gives better agreement with the profiles of Bragg reflections obtained using X-rays of PU/PAN IPN system.

References

1. Sperling, L. H. Interpenetrating Polymer Networks and Related Materials; Plenum: New York, 1981.
2. Thomas, D. A.; Sperling, L. H. In Polymer Blends; Paul, D. R., Newman, S., Eds.; Academic Press: New York, 1978; Vol. 2.
3. Frisch, H. L.; Frisch, K. C.; Klempner, D. Pure Appl Chem 1981, 53, 1557.
4. Hourston, D. J.; Zia, Y. J. J Appl Polym Sci 1983, 28, 2139.
5. Hourston, D. J.; Zia, Y. J. J Appl Polym Sci 1984, 29, 2951.
6. Hourston, D. J.; Zia, Y. J. J Appl Polym Sci 1992, 46, 973.
7. Natchimuthu, N.; Rajalingam, P.; Ganga Radhakrishnan; Francis, D. J. J Appl Polym Sci 1990, 41, 3059.
8. Hourston, D. J.; Schafer, F. U. J Appl Polym Sci 1996, 62, 2025.
9. Hourston, D. J.; Zia, Y. J. J Appl Polym Sci 1984, 29, 2963.
10. Zhang, Y.; Heath, R. J.; Hourston, D. J. J Appl Polym Sci 2000, 75, 406.
11. Zhang, L.; Ding, H. J Appl Polym Sci 1997, 64, 1393.
12. Suthar, B.; Klempner, D.; Frisch, K. C.; Petrovic, Z.; Jelcic, Z. J Appl Polym Sci 1994, 53, 1083.
13. Patel, M.; Suthar, B. Eur Polym J 1987, 23, 399.
14. Fox, R. B.; Armistead, J. P.; Roland, C. M.; Moonay, D. J. J Appl Polym Sci 1990, 41, 1281.
15. Scarito, P. R.; Sperling, L. H. Polym Eng Sci 1979, 19, 297.
16. Das, D.; Nayak, P. L.; Lenka, S. Polym Plast Tech Eng 1998, 37, 419.
17. Nayak, P.; Mishra, D. K.; Sahoo, K. C.; Pai, N. C.; Jena, P. K.; Lenka, S.; Nayak, P. L. J Appl Polym Sci 2001, 20, 1349.
18. Pavlova, M.; Draganova, M. Biomaterials 1993, 14, 1024.
19. Davaran, S.; Enterzami, A. J Bioact Compat Polym 1997, 12, 47.
20. Shin, Y. C.; Han, D. K.; Kim, Y. H.; Kim, S. C. J Biomater Sci Polym Ed 1994, 6, 195.
21. Spaans, C. J.; Belgraver, V. W.; Reinstra, D.; de-Groot, J. H.; Veth, R. P.; Pennings A. J. Biomaterials 2000, 21, 2453.
22. Wiggins, M. J., Wilkoff, B.; Anderwson, J. M.; Hiltner, A. J Biomed Mater Res 2001, 58, 302.
23. Bhunia, H. P.; Jana, R. N.; Basak, A.; Lenka, S.; Nando, G. B. J Polym Sci Part A: Polym Phys 2003, 36, 391.
24. Mallu, P.; Siddaramaiah; Somashekar, R. Bull Mater Sci 2000, 23, 413.
25. Mallu, P.; Siddaramaiah; Somashekar, R. J Appl Polym Sci 1998, 68, 1739.
26. Kumar, H.; Siddaramaiah. Novel Catalyst to Synthesize Polyurethane and its IPNs. [Submitted for Indian Patent] 2005.
27. Sperling, L. H. Macromol Rev 1977, 12, 141.
28. Muneera Begum; Siddaramaiah; Somashekarappa, H.; Somashekar, R. J Elast Plast 2004, 36, 197.
29. Athawale, V. D.; Raut, S. S. Eur Polym J 2002, 38, 2033.
30. Flory, P. J. Principles of Polymer Chemistry; Cornell University Press: New York, 1953.
31. Flory, P. J.; Rehener, J, Jr. J Chem Phys 1943, 11, 521.
32. Desai, S.; Thakore, I. M.; Sarawade, B. D.; Devi, S. Eur Polym J 2000, 36, 711.
33. Stokes, A. R. Proc Phys Soc London 1948, 61, 382.
34. Warren, B. E.; Averbach, B. L. J Appl Phys 1950, 21, 595.
35. Warren, B. E. Acta Crystallogr 1955, 8, 183.
36. Warren, B. E. X-ray Diffraction; Addison-Wesley: New York, 1969.
37. Hall, I. H.; Somashekar, R. J Appl Crystallogr 1991, 24, 1051.

38. Ribarik, R.; Ungar, T.; Gubicza, J. J Appl Crystallogr 2001, 34, 669.
39. Popa, N. C.; Balzar, D. J Appl Crystallogr 2002, 35, 338.
40. Scardi, P.; Leoni, M. Acta Crystallogr 2001, A57, 604.
41. Balzar, D. IUCr Newsletter 2002, 28, 14.
42. Somashekar, R.; Hall, I. H.; Carr, P. D. J Appl Crystallogr 1989, 22, 363.
43. Somashekar, R.; Somashekarappa, H. S. J Appl Crystallogr 1997, 30, 147.
44. Soamshekar, R.; Somashekarappa, H.; Subramanyam, G.; Prahllad, U. D. Eur Polym J 1997, 33, 963.
45. Suthar, B.; Parikh, N.; Patel, N. Polym Int 1991, 25, 173.
46. Susheela Bai; Khakhar, D. V.; Nadkarni, V. M. Polymer 1997, 38, 4319.
47. Aithal, U. S.; Aminabhavi, T. M.; Cassidy, P. E. Barrier Polymers and Structures; American Chemical Society: Washington, DC, 1990; Chapter 19, p 351.
48. Nandi, R. K.; Kuo, H. R.; Schlosberg, M.; Wissler, G.; Cohen, J. B.; Crist, B. J. J Appl Crystallogr 1984, 17, 22.
49. Press, W.; Flannery, B. P.; Teukolsky, S.; Vetterling, W. T., Eds. Numerical Recipes; Cambridge University Press: London, 1986.
50. Lee, K. G.; Barton, Jr.; Schultz, J. M. J Polym Sci Part B: Polym Phys 1995, 33, 1.